Magnetic, thermodynamic, and electrical transport properties of ternary equiatomic ytterbium compounds YbTM (T=transition metal, M=Sn and Bi)

D. Kaczorowski*
W. Trzebiatowski Institute for Low Temperature and Structure Research, Polish Academy of Sciences, P.O. Box 1410, 50-950 Wrocław 2, Poland

A. Leithe-Jasper, P. Rogl, and H. Flandorfer
Institut für Physikalische Chemie der Universität Wien, Währingerstrasse 42, A-1090 Vienna, Austria

T. Cichorek
W. Trzebiatowski Institute for Low Temperature and Structure Research, Polish Academy of Sciences, P.O. Box 1410, 50-950 Wrocław 2, Poland

R. Pietri and B. Andraka
Department of Physics, University of Florida, P.O. Box 118440, Gainesville, Florida 32611
(Received 21 April 1998; revised manuscript received 2 November 1998)

Physical behavior of several YbTM intermetallics has been studied by means of x-ray powder diffraction, magnetization, dc magnetic susceptibility, heat capacity, and electrical resistivity measurements. The compounds YbTBi with T=Cu, Ag, Au and YbTSn with T=Ag, Au, Zn were shown to be nonmagnetic due to the presence of divalent ytterbium ions. The bismuthide YbPdBi as well as the stannides YbRhSn and YbPtSn were found to exhibit localized magnetism of almost trivalent Yb ions. The electrical behavior of these three phases is characteristic of dense Kondo systems, and their low-temperature specific heat data indicate a possible heavy fermion ground state. [S0163-1829(99)12525-6]

I. INTRODUCTION

Ternary equiatomic phases of ytterbium YbTM, where T stands for a d-electron transition metal and M is an element from the IIIA, IVA or VA group of the Periodic Table, have attracted in recent years a widespread attention, mainly due to their highly unusual physical properties. Besides well-known mixed valent systems, like YbCuAl (Ref. 1) and YbPdIn,[2] the YbTM series comprises antiferromagnetically or ferromagnetically ordered Kondo lattices, e.g., YbPtGa (Ref. 3) and YbNiSn,[4] respectively. A great deal of interest has been devoted to ytterbium-based heavy fermion systems, such as antiferromagnetic YbNiAl (Ref. 5) or paramagnetic YbPdSb and YbPdBi.[6,7] The semimetallic bismuthide YbPtBi (Ref. 8) has deserved a special attention as that it displays both a low-carrier conductivity and a huge low-temperature Sommerfeld coefficient that exceeds 8 J/mol K^2.[9]

In the present paper we focus on the synthesis, structural chemistry and physical properties of several YbTM compounds, where T is either a platinum group or copper group element and M is either Sn or Bi. To the best of our knowledge, the only bismuthide that has been characterized magnetically was YbPdBi.[6,7,10] In the course of the present study a paper by Katoh *et al.* has appeared[11] that reported on a similar independent investigation on the magnetic and electrical behavior of the YbTSn stannides with T=Ag, Pt, and Au.

II. EXPERIMENTAL

Starting materials of 99.9% minimum purity were used in the form of ingots (Yb, Bi, Sn, Cu, Ag, Au), foils (Pd) or powders (Rh, Pt). Due to the high vapor pressure of ytterbium metal at elevated temperatures, synthesis of single-phase material turned out to be quite cumbersome and was achieved following two different routes. In order to benefit from the advantages of a closed system, one method was to enclose the starting materials in small cylindrical tantalum cans, which were sealed by arc-welding under pure argon. The samples, each with a total weight of about 0.5 g, were melted and, in order to attain proper homogenization, remelted in an induction furnace under continuous shaking of the crucible in a stream of high purity argon. The tantalum crucibles were then sealed in quartz tubes under vacuum and annealed at 600 °C for 7 days and finally quenched in water. The samples synthesized by this method were found to be melt homogeneously, covering large parts of the inner crucible wall in the form of a thin layer, which was usually crushed to smaller pieces when opening the crucible. Thus samples prepared by this method proved unfit for any transport measurements and were therefore mainly used for x-ray phase analysis and magnetic measurements.

In order to produce samples of well defined shapes, conventional arc-melting of 0.5 g samples under a protective argon-gas atmosphere (99.999 mass%) on a water cooled copper hearth was applied as the second method of synthesis. To achieve single-phase material usually several attempts were undertaken starting from various stoichiometries to

TABLE I. Lattice parameters for Yb*TM* bismuthides and stannides.

Compound	Space group	Structure type	Lattice parameters				Ref.
			a (nm)	*b* (nm)	*c* (nm)	*V* (nm^3)	
YbPdBi	$F\bar{4}3m$	MgAgAs	0.65934(3)			0.2863(1)	This work
			0.6547(3)			0.2806	7
			0.659			0.286	6
YbCuBi	$P6_3mc$	LiGaGe	0.45829(9)		0.7854(3)	0.1428(1)	This work
			0.4572(1)		0.7860(1)	0.1423(1)	13
YbAgBi	$P6_3mc$	LiGaGe	0.48118(4)		0.7777(2)	0.1559(1)	This work
			0.4803(1)		0.777(1)	0.1552(1)	13
YbAuBi	$F\bar{4}3m$	MgAgAs	0.6848(1)			0.3212(1)	This work
			0.6846(1)			0.3209(1)	13
YbPtSn	$P\bar{6}2m$	Fe_2P	0.7386(2)		0.39213(6)	0.1852(2)	This work
			0.7379(1)		0.3933(1)	0.1855	14
YbRhSn	$P\bar{6}2m$	Fe_2P	0.7538(1)		0.36686(8)	0.1805(1)	This work
			0.752		0.367	0.1797	14
YbAgSn	$P3m1$	CaLiSn	0.47891(8)		1.0877(4)	0.2161(1)	This work
			0.4788(1)		1.0870(1)	0.2158	15
			0.479		1.0887	0.2163	11
YbAuSn	$Pnma$	TiNiSi	0.7303(2)	0.47082(9)	0.8123(4)	0.2793(2)	This work
			0.7312	0.4716	0.8139	0.2807	11
YbZnSn	$P6_3mc$	LiGeGa	0.46514(4)		0.74732(1)	0.1399(1)	This work
			0.4649(1)		0.7476(1)	0.1399	16

compensate for the weight losses by additional amounts of Yb, Bi and Sn. The molten alloy buttons were wrapped with protective Mo-foil and sealed under vacuum in quartz ampoules followed by anneals at 600 °C for 7 days. After heat treatment the buttons were usually cut into pieces of various shapes using a diamond wire saw.

The lattice parameters were determined by leastsquares refinement of the room-temperature Guinier-Huber x-ray (Cu $K\alpha_1$) powder data, collected using 6N-germanium as an internal standard. For quantitative refinement of the atom positions, the x-ray intensities were recorded from flat specimens in a Siemens D5000 automatic powder diffractometer with Cu $K\alpha$ radiation.

Magnetic measurements were carried out in the temperature range 1.7–300 K and in magnetic fields up to 5 T employing a Quantum Design MPMS-5 SQUID magnetometer. The specific heat studies were done in the range 1–10 K using a thermal relaxation method. The electrical resistivity was measured in the temperature interval 0.08–300 K using a conventional dc four-point technique. The polycrystalline specimens were parallelepipeds cut from larger pieces with a wire saw. The electrical leads were thin copper wires contacted to the samples by tin or indium soldering. Electrical resistivity measurements below 4 K were carried out in a Cryogenics He^3-He^4 dilution refrigerator.

III. RESULTS AND DISCUSSION

A. Structure determination and structural chemistry

Although systematic search for ternary equiatomic rare earth compounds has included the usually difficult to prepare ytterbium alloys, the formation and details of crystal structures for some of the combinations are still unclear. At present more than 1300 compounds are known to form with the equiatomic formula RE(AE)*TM* (RE= rare earth, AE= alkaline earth element) adopting a variety of over 30 structure types. A successful classification was obtained by Fornasini and Merlo[12] in terms of structure maps plotting, i.e., the phases with valence electron concentration 7/3 and 8/3 per atom for the individual period number of the element *M*, each as a function of the three electronegativities on the Miedema scale, $\phi_T^* + \phi_M^* - \phi_{RE}^*$, versus the combination of the elemental radii $r_{RE}/(r_T + r_M)$.

A detailed compilation of our results and literature data on the structure types and the lattice parameters of all the alloys synthesized in this study are given in Table I. The model calculations were performed using the Lazy-Pulverix program.[17] The bismuthides YbCuBi and YbAgBi, as well as the stannide YbZnSn, were found to crystallize in the hexagonal structure of the LiGaGe-type (space group $P6_3mc$). The same structure type was established previously for YbAuSb.[18] The LiGaGe-type structure is a noncentrosymmetric ordered variant of the $CaIn_2$-type structure (space group $P6_3/mmc$) which is frequently adopted by 1:1:1 rare-earth ternaries. In Yb*TM* compounds with the $CaIn_2$-type structure, Yb is located in the $2b$ position (0,0,1/4), while *T* and *M* atoms randomly share the $4f$ position (1/3, 2/3, *z*), there occurs a fully ordered arrangement of all atoms in compounds adopting the low- symmetry structure of the LiGaGe-type.

A full atom order was also found for YbPdBi and YbAuBi crystallizing in the cubic MgAgAs-type structure (space group $F\bar{4}3m$). The stannides YbAgSn and YbAuSn adopt the hexagonal CaLiSn (space group $P3m1$) and the orthorhombic TiNiSi-type ($Pnma$) structures, respectively. In turn, the compounds YbRhSn and YbPtSn adopt the hex-

TABLE II. Crystallographic data for YbPdBi. Structure type: MgAgAs, space group $F\bar{4}3m-T_d^2$, No. 216, origin at $\bar{4}3m$, and $Z=4$; lattice parameter: $a=0.6592(1)$ nm, $V=0.2865(1)$ nm^3. B stands for the isotropic thermal parameter. Residual values: $R_I=6.99$, $R_F=6.05$, $R_p=10.2$, $R_{wp}=13.2$, and $\chi^2=4.97$. Number of reflections used in refinement: 38; scan range: $20°<2\theta<110°$; number of variables: 8.

		Positional parameters			B	
Atom	Site	x	y	z	(10^{-2} nm^2)	Occupancy
Yb	4b	1/2	1/2	1/2	1.35(7)	1
Pd	4c	1/4	1/4	1/4	1.60(6)	1
Bi	4a	0	0	0	1.29(6)	1

	Interatomic distances (nm)					
Central atom	Yb		Pd		Bi	
Ligand atoms	4 Pd	0.28545	4 Bi	0.28545	4 Pd	0.28545
	6 Bi	0.32961	4 Yb	0.28545	6 Yb	0.32961

agonal structure of the ZrNiAl-type (space group $P\bar{6}2m$) which is a fully ordered derivative of the Fe_2P-type.

The crystal structures of YbPdBi and YbPtSn were refined by means of full matrix full profile Rietveld calculations employing the PC version of the program by Wiles and Young.[19] The results shown in Table II and Table III, respectively, clearly demonstrate the complete atomic order in both compounds.

B. Physical properties

1. YbPtSn

The magnetic properties of YbPtSn are presented in Fig. 1. In agreement with the literature data[11] the compound orders antiferromagnetically at $T_N=3.5(4)$ K and exhibits Curie-Weiss behavior in the paramagnetic region. The field dependence of the magnetization, measured at 1.7 K, shows a pronounced metamagnetic transition in a field of 0.5 T. In high magnetic fields the $\sigma(B)$ variation tends to saturation and reaches at 5 T a value of 2.12(2) μ_B. Above 70 K, the inverse magnetic susceptibility is proportional to the temperature, and a least-squares fit of experimental $\chi(T)$ to the Curie-Weiss law

$$\chi(T)=\frac{C}{T-\theta_p}=\frac{1}{8}\frac{\mu_{\text{eff}}^2}{T-\theta_p} \tag{1}$$

yields the parameters: $\theta_p=9.2(8)$ K and $\mu_{\text{eff}}=4.27(2)$ μ_B (see also Table IV). This value of the effective magnetic moment is reduced with respect to a free Yb^{3+} ion value of 4.55 μ_B what suggests that the valence of ytterbium ions in YbPtSn may be slightly lower than +3. The positive sign of the paramagnetic Curie temperature indicates the presence of strong ferromagnetic interactions in this antiferromagnet. Such a situation is common in hexagonal Fe_2P-type compounds where the magnetic moments couple ferromagnetically within the (001) planes and form an antiferromagnetic sequence of these layers along the c-axis (see for example Ref. 20). At $T<70$ K the $\chi^{-1}(T)$ function of YbPtSn is curvilinear, most probably due to thermal depopulation of excited crystal-field levels.

TABLE III. Crystallographic data for YbPtSn, as derived from automatic powder diffractometer [$a=0.73856(2)$ nm, $c=0.39244(2)$ nm, $V=0.2865(1)$ nm^3, space group $P\bar{6}2m$, and $Z=3$]. B stands for the isotropic thermal parameter. Residual values: $R_I=7.43$, $R_F=10.7$, $R_p=11.4$, $R_{wp}=14.8$, and $\chi^2=10.9$. Number of reflections used in refinement: 130; scan range: $20°<2\theta<110°$; Number of variables: 11.

		Positional parameters			B	
Atom	Site	x	y	z	(10^{-2} nm^2)	Occupancy
Yb	3f	0.5969(4)	0	0	1.99(5)	1
Pt1	2d	1/3	2/3	1/2	2.53(7)	1
Pt2	1a	0	0	0	2.45(9)	1
Sn	3g	0.2597(4)	0	1/2	1.81(8)	1

	Interatomic distances (nm)							
Central atom	Yb		Pt1		Pt2		Sn	
Ligand atoms	1 Pt2	0.29767	3 Sn	0.27737	6 Sn	0.28545	2 Pt2	0.27442
	4 Pt1	0.29847	6 Yb	0.29847	3 Yb	0.29767	2 Pt1	0.27737
	2 Sn	0.31705					2 Yb	0.31705
	4 Sn	0.32681					4 Yb	0.32681
							2 Sn	0.33229

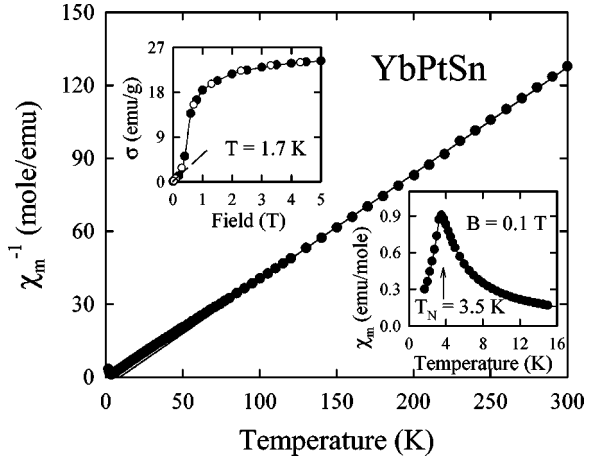

FIG. 1. Temperature dependence of the inverse molar magnetic susceptibility of YbPtSn. The solid line represents a Curie-Weiss fit with the parameters given in Table IV. The right inset shows the magnetic susceptibility at low temperatures. The upper inset displays the field variation of the magnetization, measured at 1.7 K with increasing (full circles) and decreasing (open circles) magnetic field. The dashed line marks a linear dependence below the metamagnetic transition in a field of 0.5 T.

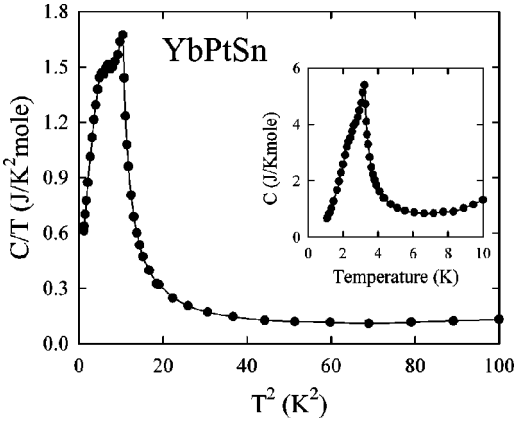

FIG. 2. The heat capacity over temperature versus temperature square for YbPtSn. The inset presents the heat capacity versus temperature. The solid lines are guides for the eye.

The above results corroborate fairly well the findings by Katoh *et al.*[11] Actually, the only significant difference between the present and previous data concerns an extra anomaly of unknown origin that was observed in $\chi(T)$ at 2.5 K by the latter authors but is absent in the $\chi(T)$ variation displayed in the inset to Fig. 1. Yet, the 2.5 K anomaly is seen in the specific heat of YbPtSn, shown in Fig. 2 as the ratio C/T versus T^2 and C versus T (the inset). This anomaly has the form of a shoulder superimposed on a much larger specific heat peak occurring at 3.5 K, which unambiguously corresponds to the antiferromagnetic phase transition. Below 2 K the specific heat can be well represented by the formula, $C/T=\gamma+\beta T^2$, with $\gamma=370(20)$ mJ/K^{2}mole and $\beta=230(6)$ mJ/K^{4}mole.

As shown in Fig. 3, the temperature dependence of the electrical resistivity of YbPtSn is of semimetallic-type with a room temperature value of about 180 $\mu\Omega$ cm and a convex character down to about 50 K. Around 20 K the $\rho(T)$ function exhibits a broad shallow minimum, and then drops rapidly at the onset of antiferromagnetic ordering at $T_N=3.5$ K. At the lowest temperatures studied (down to 50 mK) the resistivity saturates at a value of 9 $\mu\Omega$ cm that yields a residual resistivity ratio (RRR) of about 20.

The quantitative analysis of the measured ρ vs T dependence was made assuming that the Matthiessen rule is valid, i.e., that the resistivity of YbPtSn may be expressed as follows:

$$\rho(T)=\rho_0+\rho_{\rm ph}+\rho_m\,, \tag{2}$$

where ρ_0, ρ_{ph} and ρ_m stand for the residual, phonon and magnetic contributions to the total resistivity, respectively.

Having no electrical resistivity data for any non-magnetic counterpart to YbPtSn (preferably LuPtSn) it was assumed that a proper estimation of $\rho_{\rm ph}$ may be derived on the basis of the modified Bloch-Grüneissen expression

$$\rho_{\rm ph}(T)=4RT\left(\frac{T}{\Theta_D}\right)^4\int_0^{\Theta_D/T}\frac{x^5dx}{(e^x-1)(1-e^{-x})}-KT^3, \tag{3}$$

where Θ_D is the Debye temperature and R is a constant, whereas the cubic term KT^3 describes interband scattering processes.[21]

TABLE IV. Magnetic data for Yb*TM* bismuthides and stannides; AF: antiferromagnet; P: Curie-Weiss paramagnet; TIP: temperature independent paramagnet. For the meaning of the symbols see the text.

		Eq. (1)		Eq. (7)		
Compound	Magnetism	$\mu_{\rm eff}$ (μ_B)	θ_p (K)	χ_0 (emu/mole)	$\theta_p^{(i)}$ (K)	n (%)
YbPdBi	AF (?) [T_N=1 K]	4.11(5)	−3.8(9)			
YbCuBi	TIP			$1.627(8)\times10^{-4}$	−1.5(7)	1.7(3)
YbAgBi	TIP			$0.126(6)\times10^{-4}$	−1.1(8)	0.8(2)
YbAuBi	TIP			$1.719(8)\times10^{-4}$	0.8(5)	1.4(4)
YbPtSn	AF [T_N = 3.5(4) K]	4.27(2)	9.2(8)			
YbRhSn	AF (?) [T_N = 2 K]	4.51(3)	−7.0(10)			
YbAgSn	TIP			$20.914(9)\times10^{-4}$	−2.7(7)	21.0(2)
YbAuSn	TIP			$-0.021(9)\times10^{-4}$	−4.4(8)	0.1(1)
YbZnSn	TIP			$0.068(7)\times10^{-4}$	−2.1(6)	0.2(1)

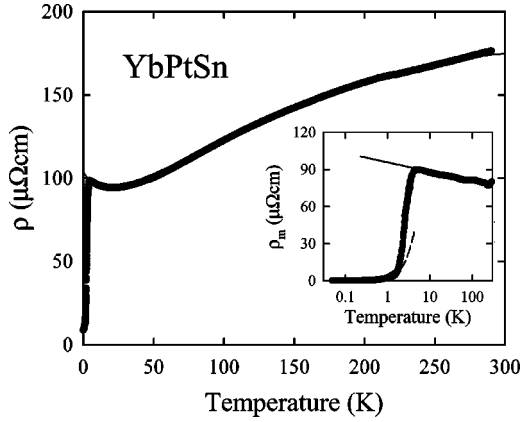

FIG. 3. Temperature dependence of the electrical resistivity of YbPtSn. The solid line is a fit of the experimental data to Eqs. (2)–(4) (see the text and Table V). The inset presents in a semilogarithmic scale the magnetic contribution to the total resistivity. The solid line marks a Kondo-like decrease of the resistivity. The dashed line shows a T^2 variation of the resistivity.

In turn, the magnetic contribution ρ_m was assumed to have in the paramagnetic region a form

$$\rho_m(T)=\rho_0^{\infty}-c_K\ln T, \tag{4}$$

where the first term accounts for the spin-disorder resistivity and the second one describes scattering of the conduction electrons via Kondo-like processes.

The solid line in Fig. 3 represents the least-squares fit of the experimental $\rho(T)$ data of YbPtSn to Eqs. (2)–(4) (for $T>5$ K), and the so-derived values of ρ_0, R, Θ_D, ρ_0^{∞} and c_K are listed in Table V. In the inset to Fig. 3, the magnetic part of the resistivity is shown in a semilogarithmic scale. It is clearly apparent from this figure that $\rho_m(T)$ of YbPtSn behaves in a Kondo-like manner above 5 K. At low temperatures ($T<1.7$ K) $\rho_m(T)$ of YbPtSn exhibits a Fermi liquid type behavior, i.e., it can be expressed as follows (note the dashed line in the inset to Fig. 3):

$$\rho_m(T)=AT^2, \tag{5}$$

with the parameter A=2.4(7) $\mu\Omega$ cm/K^2.

An enhanced γ value of 370 mJ/K^{2}mole may suggest a possibility of the coexistence in YbPtSn of a heavy fermion state and a long range antiferromagnetic order, as found in several other antiferromagnetic Kondo lattices, e.g., in isostructural YbNiAl.[5] However, the above value of γ would imply in terms of the Coqblin and Schrieffer theory[22] a Kondo temperature of about 11 K, and thus one would expect an increase in C/T below 9–10 K. Apparently no such behavior is observed in Fig. 2, and the specific heat of YbPtSn is dominated by a huge magnetic anomaly at the lowest temperatures studied. On the other hand, a similarly ''normal'' specific heat near 10 K has also been observed in the aforementioned YbNiAl, despite its large Sommerfeld coefficient $\gamma=350$ mJ/K^{2}mole, measured below T_N of 2.5 K.[5] Such a behavior of the specific heat can be understood if one takes into account that as in many other heavy fermion antiferromagnets, the Kondo temperature in both compounds drastically changes when passing through T_N. Indeed, for YbNiAl the Kondo temperature determined in the paramagnetic region is only about 3 K.[5] It seems likely that a similar situation may occur also for YbPtSn, as impled by many similarities between the two compounds. In this context it is worthwhile noting that the suggested scenario of the coexistence of heavy fermion liquid and magnetic order is consistent with other measured bulk characteristics of YbPtSn. First, the measured value of the coefficient β in the cubic temperature contribution to the specific heat reproduces rather well the magnitude of T_N, calculated with the assumption of a linear spin-wave dissipation relation.[23] Then, the low temperature behavior of the resistivity, observed over more than a decade of temperature values (for $0.06<T<1.7$ K), is given by the quadratic term with a strongly enhanced A coefficient, comparable to that found in many heavy fermion systems. According to an experimental study of Kadowaki and Woods,[24] A is proportional to the square of the linear coefficient of the electronic specific heat via the universal relation: $A/\gamma^2\simeq 10^{-5}$ $\mu\Omega$ cm mole^{2}K^4/mJ^2. This ratio, being about 20 times larger than that characteristic of simple metals and transition metals, is often considered as an important hallmark of heavy fermions. Although its almost universal value has never been fully explained, theoretical arguments by Takimoto and Moriya[25] suggest that it reflects strongly correlated nature of conduction electrons. For YbPtSn the ratio of A and γ^2, where γ is extrapolated from the lowest temperature specific heat data, is about 50 % larger than the above universal value, but it is close to that found in many well established heavy fermion antiferromagnets, such as $CePb_3$,[26] $CaAl_2$,[27] $CeAuAl_3$,[28] and $CePd_2In$.[29] Interestingly, in all these compounds T_N is of the order 1 K. This coincidence may further suggest an antiferromagnetic heavy fermion nature of YbPtSn. However, we stress that in order to fully conclude this coexistence, additional complementary experiments, such as measurements of the magnetoresistance above T_N as well as very low temperature specific heat studies (down to 100 mK) are required.

2. YbRhSn

As is apparent from Fig. 4, also YbRhSn exhibits well localized magnetism due to the presence of stable Yb^{3+} ions. The effective magnetic moment derived from a Curie-Weiss fit [Eq. (1)] of experimental $\chi(T)$ above 30 K is almost equal to the value expected for the $4f^{13}$ configuration being 4.51(3) μ_B. The paramagnetic Curie temperature amounts to −7(1)

TABLE V. Electrical resistivity for YbPtSn and YbRhSn. For the meaning of the symbols, see the text.

Compound	ρ_0 ($\mu\Omega$ cm)	R ($\mu\Omega$ cm/K)	Θ_D (K)	$K\times10^6$ ($\mu\Omega$ cm/K^3)	ρ_0^{∞} ($\mu\Omega$ cm)	c_K ($\mu\Omega$ cm)	A ($\mu\Omega$ cm/K^2)
YbPtSn	9(2)	0.43(2)	204(2)	1.4(3)	94(3)	2.9(4)	2.4(7)
YbRhSn	85(2)	0.46(3)	199(1)	0.9(2)	33(4)	3.0(3)	6.8(3)

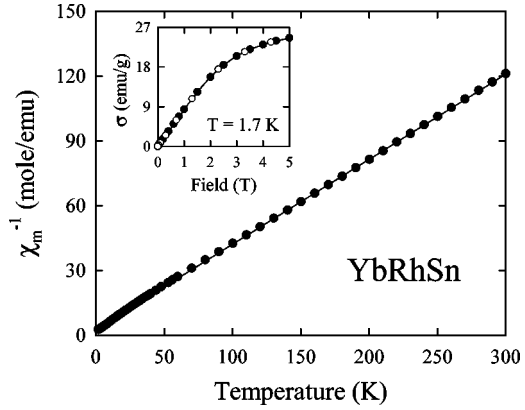

FIG. 4. Temperature dependence of the inverse molar magnetic susceptibility of YbRhSn. The solid line represents a Curie-Weiss fit with the parameters given in Table IV. The inset shows the field variation of the magnetization, measured at 1.7 K with increasing (full circles) and decreasing (open circles) magnetic field.

K. A slight deviation of the inverse susceptibility from a straight line behavior, observed at lower temperatures, arises presumably from crystal field interactions.

From the low-temperature variation of the magnetic susceptibility and the field dependence of the magnetization measured at 1.7 K (see the insets to Fig. 4) one would conclude that YbRhSn remains paramagnetic down to the lowest temperatures studied. However, the specific heat results, shown in Fig. 5, contradict this presumption. The C versus T variation has two anomalies, a less pronounced feature at 2 K and a more pronounced one at 1.5 K, below which the specific heat starts to decrease with decreasing temperature. In turn, the C/T ratio increases continuously from about 9 K down to 1.5 K and it is only slightly reduced between 1.5 and 1 K. Interestingly, the total entropy (including phonon contribution) that is removed in the interval 1–10 K is 4.6 J/Kmole, i.e., about $0.8R\ln 2$. At 10 K, C/T reaches only about 80 mJ/K^{2}mole and can be almost completely accounted for by a phonon contribution. Therefore, it is doubtful that an additional paramagnetic entropy associated with the ground state doublet is removed above 10 K. The entropy consideration implies very large values of C/T below 1 K, which would be consistent with our data.

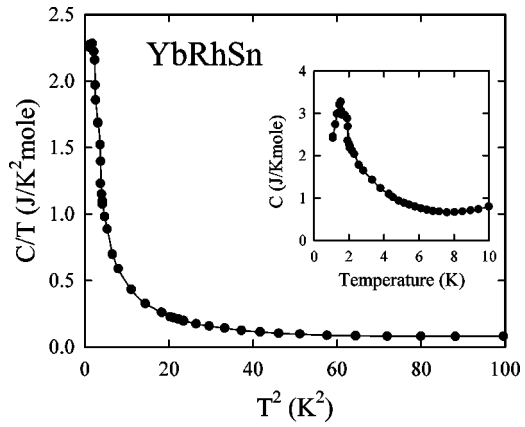

FIG. 5. The heat capacity over temperature versus temperature square for YbRhSn. The inset presents the heat capacity versus temperature. The solid lines are guides for the eye.

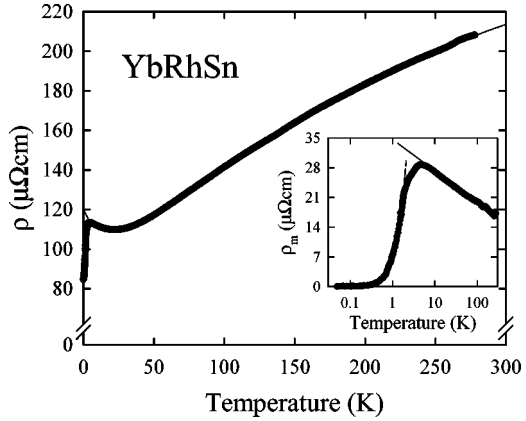

FIG. 6. Temperature dependence of the electrical resistivity of YbRhSn. The solid line is a fit of the experimental data to Eqs. (2)–(4) (see the text and Table V). The inset presents in a semilogarithmic scale the magnetic contribution to the total resistivity. The solid line marks a Kondo-like decrease of the resistivity. The dashed line shows a T^2 variation of the resistivity.

The temperature dependence of the electrical resistivity of YbRhSn is displayed in Fig. 6. The overall shape of the $\rho(T)$ curve is very similar to that obtained for YbPtSn. The room temperature resistivity equals to about 215 $\mu\Omega$ cm, yet the RRR value is only 2.5 here. Interestingly, a minimum in $\rho(T)$ around 25 K is followed by a rapid decrease in the resistivity below 5 K resembling the behavior of antiferromagnetic YbPtSn. However, in this case the kink in $\rho(T)$ cannot be attributed to the magnetic phase transition as YbRhSn orders below 2 K. Any suspicion that the observed anomaly is due to the presence of some free tin that becomes superconducting at low temperatures can be ruled out because no indication of such a transition is seen neither in the heat capacity (see Fig. 5) nor in the dc magnetic susceptibility measured in weak fields (not shown). Moreover, upon applying magnetic field, the resistivity of YbRhSn measured at 4.2 K decreases continuously.[30] Hence, it seems likely that the observed low-temperature behavior of the resistivity of YbRhSn may be associated with the onset of the coherence effect or/and with the manifestation of an interplay of crystal-field and Kondo-like interactions.

The numerical analysis of $\rho(T)$ for YbRhSn, performed using the approach described above, yielded the parameters ρ_0, R, Θ_D, ρ_0^{∞}, c_K and A given in Table V. The solid line in Fig. 6 is the fit of the experimental data to Eqs. (2)–(4), and the inset to this figure presents the magnetic part of the resistivity in a semilogarithmic scale. The solid line in the inset marks a pronounced Kondo-like decrease of the resistivity and the dashed line indicates the region where a T^2 behavior is observed (for $0.06<T<1.9$ K), with a strongly enhanced A coefficient of 6.8(3) $\mu\Omega$ cm/K^2. It is worthwhile noting that this value of A is even larger than that found for YbPtSn, which points to the possibility of a heavy fermion ground state also in YbRhSn.

3. YbAgSn, YbAuSn, YbZnSn

The magnetic properties of YbAuSn and YbZnSn are presented in Figs. 7 and 8, respectively. The small magnitude of the magnetic susceptibility of both compounds in the whole

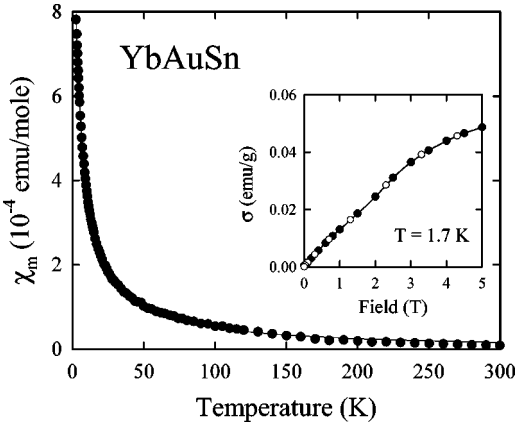

FIG. 7. Temperature dependence of the molar magnetic susceptibility of YbAuSn. The solid line represents a fit of the experimental data to Eq. (6) with the parameters given in Table IV. The inset shows the field variation of the magnetization, measured at 1.7 K with increasing (full circles) and decreasing (open circles) magnetic field.

temperature range studied, as well as low values of their magnetization measured at 1.7 K, unambiguously indicate a nonmagnetic ground state with ytterbium ions exhibiting a $4f^{14}$ configuration. This finding corroborates the results obtained previously for YbAuSn by Katoh *et al.*[11] Pronounced tails in $\chi(T)$, observed for these two ternaries at low temperatures, may be attributed to a small amount of Yb^{3+} ions present in the samples in the form of paramagnetic impurities, most probably some ytterbium oxides or/and hydroxides. The amount of these admixtures can be estimated assuming that their contribution to the measured susceptibility may be expressed in the form of an extra Curie-Weiss term with the Curie constant $C^{(i)}$ being a fraction n of the value characteristic of a free Yb^{3+} ion $C_{Yb^{3+}}=(8\times4.53)^{1/2}=6.02$. Within this approach crystal-field effect acting on a Yb^{3+} ion is neglected. Thus, the total susceptibility is approximated by

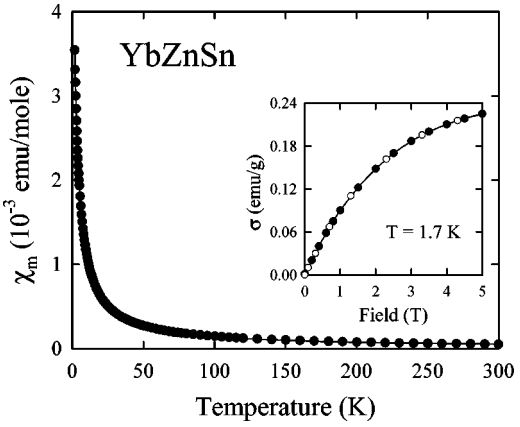

FIG. 8. Temperature dependence of the molar magnetic susceptibility of YbZnSn. The solid line represents a fit of the experimental data to Eq. (6) with the parameters given in Table IV. The inset shows the field variation of the magnetization, measured at 1.7 K with increasing (full circles) and decreasing (open circles) magnetic field.

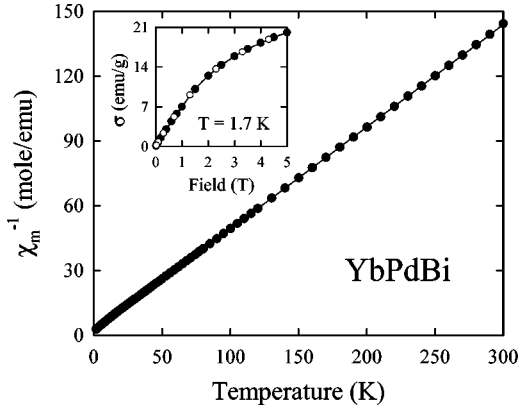

FIG. 9. Temperature dependence of the inverse molar magnetic susceptibility of YbPdBi. The solid line represents a Curie-Weiss fit with the parameters given in Table IV. The inset shows the field variation of the magnetization, measured at 1.7 K with increasing (full circles) and decreasing (open circles) magnetic field.

$$\chi(T)=\chi_0+\frac{C^{(i)}}{T-\theta_p^{(i)}}=\chi_0+\frac{nC_{\mathrm{Yb}^{3+}}}{T-\theta_p^{(i)}}, \tag{6}$$

where χ_0 is the Pauli-like intrinsic susceptibility of the 1:1:1 compound and $\theta_p^{(i)}$ stands for the paramagnetic Curie temperature of an impurity. The results of least-squares fitting the experimental data of YbAuSn and YbZnSn to Eq. (6) are given in Table IV. In both samples the amount of free Yb^{3+} ions was estimated to be as low as 0.1–0.2 % , which explains the absence of any impurity lines on their x-ray patterns. The intrinsic magnetic susceptibility of both stannides is of the order of 10^{-6}-10^{-5} emu/mole, but it is negative for YbAuSn and positive for YbZnSn. Nevertheless, the above result clearly confirms a divalent nature of ytterbium ions in these two compounds.

A nonmagnetic ground state is also most probably realized in YbAgSn because the magnetic susceptibility of this compound behaves in a similar manner to that of YbAuSn and YbZnSn. Yet, the numerical analysis of $\chi(T)$ in terms of Eq. (6) gives in this case a rather large impurity contribution (see Table IV). Nevertheless, the temperature independent paramagnetism in YbAgSn was also claimed by Katoh *et al.*[11]

4. YbPdBi

As indicated by its temperature- and field-dependent magnetic behavior, YbPdBi does not order magnetically down to 1.7 K (see Fig. 9). In the whole temperature range studied the magnetic susceptibility follows a Curie-Weiss law with the parameters $\theta_p=-3.8(9)$ K and $\mu_{\mathrm{eff}}=4.11(5)\ \mu_B$. This effective magnetic moment is slightly reduced with respect to the value expected for a free Yb^{3+} ion (4.54 μ_B), which suggests that the ytterbium atoms in YbPdBi may have some tendency to valence fluctuations. Previously, intermediate-valent character for this compound was claimed by Dhar *et al.*[6] because of a reduced μ_{eff} and a considerable deviation of the cubic lattice parameter from the extrapolation based on the lanthanide contraction along the REPdBi series (see also Ref. 31).

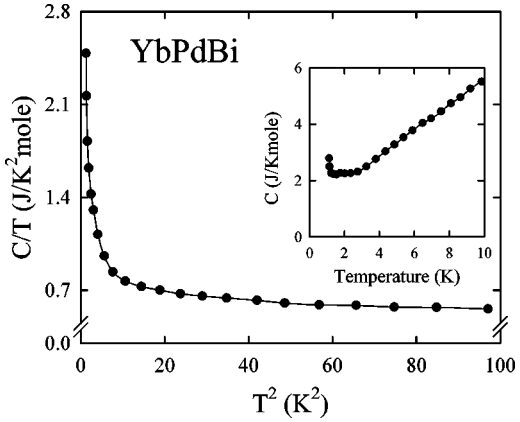

FIG. 10. The heat capacity over temperature versus temperature square for YbPdBi. The inset presents the heat capacity versus temperature. The solid lines are guides for the eye.

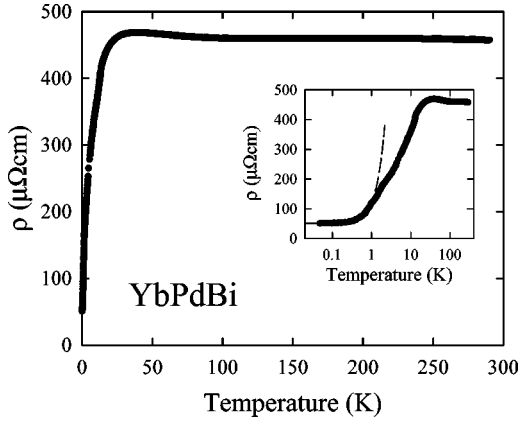

FIG. 11. Temperature dependence of the electrical resistivity of YbPdBi. The inset displays the resistivity versus temperature in a semilogarithmic scale. The dashed line shows a T^2 variation of the resistivity.

Dhar *et al.* measured also the heat capacity of YbPdBi, and from the results concluded on a heavy-fermion character of its electronic ground state.[6] Their specific heat data, plotted in the form C/T versus T^2, were reminiscent of heavy-fermion behavior: they showed a sharp upturn at low temperatures and reached as large value as 1 J/K^{2}mole at 2 K, the lowest temperature obtained. In Fig. 10, our low-temperature heat capacity of YbPdBi, measured down to 1.2 K, is presented. In agreement with the previous results the ratio C/T is larger than 500 mJ/K^{2}mole at all temperatures studied. Moreover, the observed rise in C/T continues down to the lower limit of our measurement, exceeding at this temperature a value of 2.5 J/K^{2}mole. Thus, one would conclude that YbPdBi is indeed a strongly correlated electron system with considerably enhanced effective electronic masses. However, an inspection of the specific heat itself (see the inset to Fig. 10) shows that this interpretation is not correct—a sharp increase in $C(T)$ below 1.5 K and its huge values are obvious signatures of a magnetic phase transition taking place just below the lowest temperature measured. A small anomaly in the $C(T)$ variation observed here at 1.9 K is most probably due to the presence in the sample of some small amount of YbPd which orders antiferromagnetically at this temperature.[32]

The occurrence of a magnetic phase transition in YbPdBi was explicitly evidenced in a more recent work by LeBras *et al.*[10] The latter authors measured the specific heat down to 0.5 K and found a clear λ-type anomaly at 1 K. Moreover, in the dc magnetic susceptibility they observed at this temperature a change in the curvature of $\chi(T)$ into a ferromagnetic-like convex one, and from ^{170}Yb Mössbauer spectroscopy measurements they determined the saturated Yb moment of 1.25 μ_B. Interestingly, the entropy released by the magnetic transition was estimated to be 0.4Rln2 at 1.3 K, i.e., much smaller than expected for a doublet ground state. Also the measured peak value of the $4f$-derived specific heat $C_{4f}(1K)=3.1$ J/Kmole was much smaller than expected for a second-order transition for a Kramers doublet (12.5 J/Kmole). This considerable reduction in both characteristics was ascribed to a Kondo screening effect. The Kondo temperature was estimated to be of the order of 1 K.

A clear Kondo behavior in YbPdBi is apparent from Fig. 11, which shows the temperature variation of the electrical resistivity. At ambient temperatures the resistivity exhibits a negative temperature coefficient, goes through a broad maximum centered at about 25 K, and then drops rapidly at low temperatures, finally saturates below 0.5 K (see the inset to Fig. 11). The maximum in $\rho(T)$ may arise due to the onset of coherence among the Yb ions but it may also reflect an interplay of Kondo and crystal-field interactions (see below). The magnetic phase transition manifests itself as a small kink in $\rho(T)$ and a sharp minimum in the temperature derivative of the resistivity. Below 1 K, the resistivity exhibits a T^2-dependence with the coefficients ρ_0 and A [see Eqs. (2) and (5)] equal to 51(2) $\mu\Omega$ cm and 70(3) $\mu\Omega$ cm/K^2, respectively. This huge value of A is among the largest ever reported for any materials, including heavy fermion systems. Unfortunately, no experimental information on the Sommerfeld coefficient in YbPdBi at the lowest temperatures is known. Although Dhar *et al.*[6] has determined from their high temperature ($13<T<20$ K) specific heat data an enhanced γ value of 470 mJ/mole K^2, LeBras *et al.* showed in Ref. 10 that almost all specific heat in this temperature region can be accounted for by the Schottky anomaly. In turn, the latter authors obtained for the C_{4f}/T ratio a value of about 1.8 J/mole K^2 at 0.5 K, the lowest temperature measured, but no attempt has been made to derive the $\gamma(0)$ value. Such a determination would be difficult and not very reliable due to the low value of T_N.

The ^{170}Yb Mössbauer absorption spectroscopy investigations allowed LeBras *et al.*[10] to conclude that the point symmetry of Yb ions in YbPdBi is lower than cubic. This symmetry lowering was ascribed by the latter authors to a local static Jahn-Teller effect within the Γ_8 cubic quartet. Thus, the crystal-field level scheme of the Yb^{3+} ion would consist of four Kramers doublets. Such a level scheme, with the energies of excited states 23, 80, and 90 K, is compatible with the inelastic neutron scattering data,[33] and was used in Ref. 10 for successful interpreting the Mössbauer spectra and the high-temperature specific heat results. Moreover, the maximum in the electrical resistivity occurring at about 25 K (see Fig. 11) may be associated with the thermal population of the first excited doublet in the presence of the Kondo effect, whereas the total crystal field splitting of about 90 K may explain the formation near this temperature of a charac-

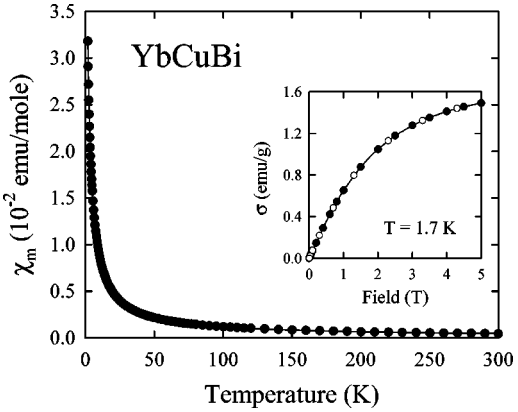

FIG. 12. Temperature dependence of the molar magnetic susceptibility of YbCuBi. The solid line represents a fit of the experimental data to Eq. (6) with the parameters given in Table IV. The inset shows the field variation of the magnetization, measured at 1.7 K with increasing (full circles) and decreasing (open circles) magnetic field.

teristic negative minimum in the temperature variation of the thermoelectric power.[7] However, as pointed out by LeBras *et al.*,[10] the proposed crystal-field level scheme cannot account for the enhanced contribution to the $4f$-derived specific heat in the vicinity of 10 K. Therefore, it seems likely that the behavior of C/T does reflect the formation in YbPdBi of a heavy fermion state which coexists at the lowest temperatures with a long range magnetic ordering. This hypothesis is now supported by our resistivity data but further studies at very low temperatures are needed in order to reliably conclude on this point.

5. YbCuBi, YbAgBi, YbAuBi

As shown in Figs. 12–14, all three 1:1:1 bismuthides which contain a $d^{10}-$type noble metal were found to be nonmagnetic with ytterbium ions exhibiting a $4f^{14}$ ground state. Pronounced tails in $\chi(T)$, observed for these compounds at low temperatures, may be attributed to some small amount of Yb^{3+} ions present in the samples in the form of

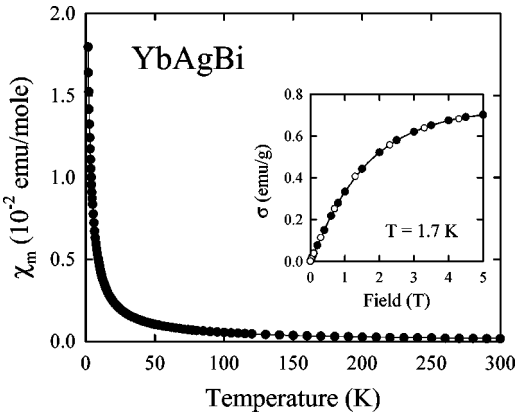

FIG. 13. Temperature dependence of the molar magnetic susceptibility of YbAgBi. The solid line represents a fit of the experimental data to Eq. (6) with the parameters given in Table IV. The inset shows the field variation of the magnetization, measured at 1.7 K with increasing (full circles) and decreasing (open circles) magnetic field.

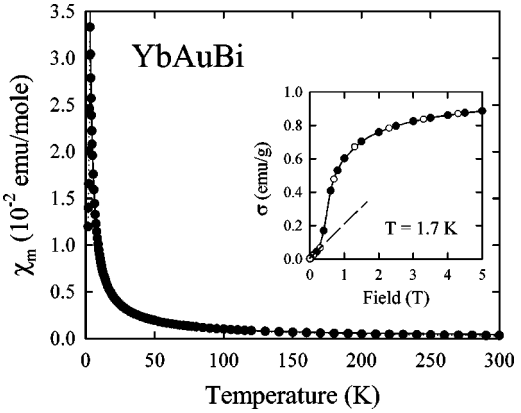

FIG. 14. Temperature dependence of the molar magnetic susceptibility of YbAuBi. The solid line represents a fit of the experimental data to Eq. (6) with the parameters given in Table IV. The dotted line is a guide for the eye, showing the antiferromagnetic maximum due to the presence of Yb_2O_3 impurity. The inset presents the field variation of the magnetization, measured at 1.7 K with increasing (full circles) and decreasing (open circles) magnetic field. The dashed line displays a metamagnetic transition in Yb_2O_3 antiferromagnet.

paramagnetic impurities. In the case of YbAuBi a sharp maximum in the susceptibility occurring at $T_N = 3.2(4)$ K, together with a salient metamagnetic-like transition observed in the $\sigma(B)$ dependence (see the inset to Fig. 14), allow to ascribe the low temperature behavior of $\chi(T)$ measured on this specimen to antiferromagnetic Yb_2O_3. For the other two compounds it is impossible to assign any particular foreign phase as they remain paramagnetic down to the lowest temperatures studied. However, because of extreme sensitivity of the ternary bismuthides to air and moisture, it seems likely that the impurities formed were some ytterbium oxides or/and hydroxides.

In a manner similar to that described for the stannides, the experimental $\chi(T)$ data obtained for YbCuBi, YbAgBi, and YbAuBi were least-squares fitted to Eq. (6) and the results of this analysis are given in Table IV. In the bismuthide samples the amount of paramagnetic impurities was found to be slightly larger than in the stannides, about 1–2 %. The intrinsic susceptibility χ_0 for all three compounds was of paramagnetic type with magnitudes of the order of 10^{-5}-10^{-4} emu/mole.

The above magnetic characteristics of YbCuBi, YbAgBi and YbAuBi correspond well with the results of electrical resistivity measurements reported by Merlo *et al.*[34] All three compounds were established to be metals, and the electrical resistivity of YbAgBi and YbAuBi was found to be fully describable by the sum of the residual resistivity and modified Bloch-Grüneissen [see Eq. (4)] terms. It is worthwhile noting at this place that the parameters R, Θ_D and K derived by the latter authors for these two bismuthides have the same order of magnitude as those values estimated in the present work for YbPtSn and YbRhSn. This coincidence may be taken as a proof of the correctness of the approach applied in these two independent studies. In the case of YbCuBi the resistivity measured in Ref. 34 behaved in a more complicated manner, ascribed to the presence of microcracks and/or some anomalous electronic band structure effects.

IV. CONCLUSIONS

A great interest in ytterbium-based compounds comes from the fact that Yb can exhibit two valence states, that correspond to two almost degenerate $4f$ configurations: nonmagnetic $4f^{14}(Yb^{2+})$ and magnetic $4f^{13}(Yb^{3+})$. Due to this feature Yb is usually considered as a ''hole'' counterpart to Ce that also shows two terminal electronic configurations, which are closely spaced in energy: magnetic $4f^1(Ce^{3+})$ and nonmagnetic $4f^0(Ce^{4+})$. It is commonly believed that the main mechanism determining the ground state behavior in cerium and ytterbium intermetallics is the interaction between $4f$ electrons and *s*, *p*, and *d* electrons of neighboring ligands. This so-called $f-spd$ hybridization tends to reduce the $4f$-level occupation number and thus destabilize the magnetic state of cerium ion or the nonmagnetic state of ytterbium ion. As a result of the valence instability a number of interesting phenomena develops, like Kondo effect, heavy-fermion behavior, spin fluctuations, intermediate valence. However, in contrast to cerium intermetallics where these spectacular effects are observed quite frequently, only few ytterbium systems are known where a pronounced Kondo effect and the formation of heavy fermion state occur. This is certainly because of a stronger localization of the $4f$ wave functions (smaller spatial extent) in Yb^{3+} ion as compared to that in Ce^{3+} ion.[35]

For weak f-spd hybridization the $4f^{14}$ configuration is rather stable and therefore most ytterbium intermetallics contain Yb^{2+} ions.[36] The compounds studied in the present paper are here the best examples. The bismuthides YbCuBi, YbAgBi, and YbAuBi as well as the stannides YbAgSn, YbAuSn, and YbZnSn have been shown to be temperature independent paramagnets due to the presence of nonmagnetic Yb^{2+} ions. Indeed, the $4f$-ligand hybridization is expected to be very weak in all these ternaries mainly because of filled *d*-shell of the transition metal component. In such a situation cerium compounds usually exhibit well localized magnetism due to the presence of stable Ce^{3+} ions, as is the case of the cerium-based counterparts CeAgSn and CeAuSn, which order antiferromagnetically at low temperatures.[37]

Upon replacing a noble-metal element by an element with unfilled *d*-shell it is expected that the $4f$-ligand hybridization increases in its strength, and thus a valence may change to the higher state. For example, in CeRhSn the $4f$-shell is indeed unstable and the compound exhibits the properties characteristic of intermediate valent systems.[38] In turn, in the case of YbRhSn, studied in the present paper, a rather well localized magnetism due to the presence of almost trivalent ytterbium ions is observed. A similar valence change occurs upon replacing a noble-metal element by Pt (YbPtSn) and Pd (YbPdBi). All three compounds order magnetically at low temperatures and their overall electrical properties are characteristic of Kondo lattices. Moreover, their low-temperature specific heat data indicate a possible heavy fermion ground state.

A qualitative analysis of the influence of the f-d and f-p hybridization on the magnetic behavior in YbTM intermetallics can be made by comparing the properties of isostructural compounds with different *T* and *M* elements, respectively. For example, let us consider the YbTM series of compounds crystallizing with the cubic MgAgAs-type structure. If *T* = Pd is kept, only two such ytterbium ternaries are known to form, namely YbPdBi and YbPdSb. Interestingly, both these compounds have rather similar magnetic properties, which may suggest that the hybridization effect has there a similar character and magnitude. Also, the specific heat values for YbPdBi and YbPdSb, determined in the temperature range 13–20 K, are alike and approximately equally enhanced. Below 10 K C/T exhibits a pronounced upturn in both compounds.[6] Depending on the preparation conditions the YbPdSb compound either remains paramagnetic down to 0.01 K, showing only short-range dynamic correlations of antiferromagnetic character below 5 K, or exhibits a first-order phase transition to long-range antiferromagnetism below 1 K.[39] In both cases YbPdSb was characterized as a Kondo lattice with RKKY exchange interactions, which are of the same order of magnitude as the Kondo temperature, thus being located very close to the magnetic-nonmagnetic instability on the Doniach's diagram. Very similar magnetic behavior in YbPdSb and YbPdBi can be easily understood taking into account that upon replacing Sb by Bi the f-d hybridization due to the transition metal atom is probably unaltered, while the f-p hybridization is also hardly modified, as both *M* elements are pnictogens with the same p^3 configuration of their outer electronic shell.

It is worthwhile noting at this place that another YbPd*M* ternary phase, but with *M* = In, is an intermediate valence system.[2] However, YbPdIn crystallizes with a hexagonal structure of the ZrNiAl-type, and thus cannot be directly related to the two cubic compounds discussed above. It is because the different ground state properties in YbPdIn may be caused to some extent also by a different site symmetry of the ytterbium atom.

Now, let us turn to YbTBi (*T*=Au, Pd and Pt) compounds, which adopt the MgAgAs-type structure. As already discussed above, in YbAuBi both the f-d and f-p interactions are presumably weak and the Yb ion exhibits the nonmagnetic divalent state. In YbPdBi and YbPtBi the f-p hybridization is supposed to have a similar magnitude as in YbAuBi but the strength of the f-d hybridization considerably increases. This latter effect results in a dramatic change in the magnetic behavior. Both YbPdBi and YbPtBi (Ref. 9) contain almost trivalent ytterbium ions, as indicated, e.g., by a Curie-Weiss character of the magnetic susceptibility with $\mu_{\rm eff}$ close to 4.54 μ_B, and order magnetically at low temperatures (1 and 0.4 K, respectively). The Pt-based bismuthide is a well established semimetallic heavy-fermion system ($\gamma \approx 8$ J/mol K^2) with very low carrier concentration.[9] The ground-state properties of this compound are governed by three competing energy scales, related to the magnetic exchange, the crystal-field splitting and the Kondo-screening effect, respectively. As a result of the concerted action of these three interactions, all of order 1 K, an antiferromagnetic ordering develops with strongly reduced local moment (0.1 μ_B), and simultaneously below T_N a superzone gap is formed.[8] The Kondo effect in the electrical resistivity of YbPdBi, is even more pronounced than that in YbPtBi. Also the energy associated with the crystal-field effect in YbPdBi is much larger than that for the Pt-containing counterpart (see above). These differences arise presumably due to a different strength of the f-d hybridization in the two compounds. Thus, in view of the above analysis of the effect of

varying the interactions of ytterbium $4f$-electrons with p- and d-electrons of neighboring ligands along the YbPdM and YbTBi series, respectively, when keeping the structural factors constant, one may conclude that the main mechanism which determines the magnetic behavior of the compounds studied is most probably just the f-d hybridization.

Finally, it is worth to comment on the complex low-temperature magnetic behavior in YbRhSn and YbPtSn, evidenced by multiple phase transitions found in heat capacity studies. The formation of a complex magnetic ground state is characteristic of many cerium and ytterbium compounds crystallizing with orthorhombic or hexagonal structures where the magnetic exchange interactions are strongly anisotropic and heavily frustrated because of the topology of the crystal lattice. In CePtSn and CePtAl, which adopts the orthorhombic ε-TiNiSi-type crystal structure, the low-temperature magnetic properties with two and three successive magnetic phase transitions, respectively, are governed by an interplay between strong crystal-field effects and competing magnetic exchange interactions between Ce-Ce nearest and next-nearest neighbors.[40,41] A similar mechanism was recently proposed to interpret a complexity of the magnetic ground states occurring in isostructural ytterbium dense Kondo systems: antiferromagnetic YbPtAl[42] and ferromagnetic YbNiSn.[43] The stannides YbRhSn and YbPtSn crystallize in the hexagonal ZrNiAl-type structure, where the development of magnetic frustration is even more likely due to a triangular coordination symmetry of the magnetic ions. Such a geometrical frustration in triangular lattice has been shown to be responsible for the complexity of magnetic structures and phase transitions in antiferromagnetic TbNiAl.[44] In this case two nearest neighbors to a given magnetic ion are themselves nearest neighbors and antiferromagnetic coupling among them cannot be completely satisfied. This effect gives rise to the splitting of the system of equivalent magnetic moments into two different types of antiferromagnetically ordered moments which behave separately. As a result, a complex phase diagram with several phase transitions is observed. In view of the magnetic data obtained in the present work it seems likely that a similar situation may occur in YbRhSn and YbPtSn. Hence, both compounds are promising candidates for studying complex magnetic structures by neutron diffraction. Moreover, ytterbium is a suitable NMR and Mössbauer nucleus and therefore further studies employing these two microscopic techniques is also of great interest.

ACKNOWLEDGMENTS

The authors gratefully acknowledge the support of the Austrian-Polish Scientific-Technical exchange program (project N6). The research was in part supported by the Austrian FFWF under Grant No. P9707. In the initial stage of the work a series of samples was prepared at the Dipartimento de Chimica e Chimica Industriale, Sezione di Chimica Inorganica e Metallurgia at the University of Genova, Italy. The help and interest of Professor A. Saccone and Professor R. Ferro are appreciated. The work at Florida was supported by the National Science Foundation, Grant No. DMR-9400755.

*Author to whom correspondence should be addressed.

[1] W. C. M. Mattens, R. A. Elenbas, and F. R. de Boer, Commun. Phys. **2**, 147 (1977).

[2] S. Cirafici, A. Palenzona, and F. Canepa, J. Less-Common Met. **107**, 179 (1985).

[3] D. T. Adroja, B. D. Rainford, S. K. Malik, M. Gailloux, and K. A. Gschneidner, Jr., Phys. Rev. B **50**, 248 (1994).

[4] P. Bonville, P. Bellot, J. A. Hodges, P. Imbert, G. Jéhanno, G. Le Bras, J. Hammann, L. Leylekian, G. Chevrier, P. Thuéry, L. D'Onofrio, A. Hamzic, and A. Barthélémy, Physica B **182**, 105 (1992).

[5] C. Schank, G. Olesch, J. Köhler, U. Tegel, U. Klinger, J. Diehl, S, Klimm, G. Sparn, S. Horn, C. Geibel, and F. Steglich, J. Magn. Magn. Mater. **140-144**, 1237 (1995); J. Diehl, H. Davideit, S. Klimm, U. Tegel, C. Geibel, F. Steglich, and S. Horn, Physica B **206&207**, 344 (1995).

[6] S. K. Dhar, N. Nambudripad, and R. Vijayaraghavan, J. Phys. F **18**, L41 (1988).

[7] F. G. Aliev, G. I. Pak, and T. M. Shkatova, Fiz. Tverd. Tela (Lenningrad) **31**, 244 (1989) [Sov. Phys. Solid State **31**, 1615 (1989)].

[8] M. F. Hundley, J. D. Thompson, P. C. Canfield, and Z. Fisk, Phys. Rev. B **56**, 8098 (1997); P. C. Canfield, R. Movshovich, R. A. Robinson, J. D. Thompson, Z. Fisk, W. P. Beyermann, A. Lacerda, M. F. Hundley, R. H. Heffner, D. E. MacLaughlin, F. Trouw, and H. R. Ott, Physica B **197**, 101 (1994), and references cited therein.

[9] Z. Fisk, P. C. Canfield, W. P. Beyermann, J. D. Thompson, M. F. Hundley, H. R. Ott, E. Felder, M. B. Maple, M. A. Lopez de la Torre, P. Visani, and C. L. Seaman, Phys. Rev. Lett. **67**, 3310 (1991).

[10] G. LeBras, P. Bonville, J. A. Hodges, J. Hammann, M. J. Besnus, G. Schmerber, S. K. Dhar, F. G. Aliev, and G. André, J. Phys.: Condens. Matter **7**, 5665 (1995).

[11] K. Katoh, T. Takabatake, A. Minami, I. Oguro, and H. Sawa, J. Alloys Compd. **261**, 32 (1997).

[12] M. L. Fornasini and F. Merlo, J. Alloys Compd. **219**, 63 (1995).

[13] F. Merlo, M. Pani, and M. L. Fornasini, J. Alloys Compd. **166**, 319 (1990).

[14] A. E. Dwight, W. C. Harper, and C. W. Kimball, J. Less-Common Met. **30**, 1 (1973).

[15] F. Merlo, M. Pani, and M. L. Fornasini, J. Alloys Compd. **232**, 289 (1996); D. Mazzone, D. Rossi, R. Marazza, and R. Ferro, J. Less-Common Met. **80**, P47 (1981).

[16] F. Merlo, M. Pani, and M. L. Fornasini, J. Alloys Compd. **221**, 280 (1995).

[17] K. Yvon, W. Jeitschko, and E. Parthé, J. Appl. Crystallogr. **10**, 73 (1977).

[18] H. Flandorfer, K. Hiebl, C. Godart, P. Rogl, A. Saccone, and R. Ferro, J. Alloys Compd. **256**, 170 (1997).

[19] D. B. Wiles and R. A. Young, J. Appl. Crystallogr. **14**, 151 (1981).

[20] G. Ehlers and H. Maletta, Z. Phys. B **101**, 317 (1996).

[21] N. F. Mott and H. Jones, *The Theory of the Properties of Metals and Alloys* (Oxford University Press, New York, 1958), p. 240.

[22] B. Coqblin and J. R. Schrieffer, Phys. Rev. **185**, 847 (1969).

[23] S. V. Vonsovskii, *Magnetism* (John Wiley and Sons, New York, 1974), Vol. 2, p. 876.

[24] K. Kadowaki and S. B. Woods, Solid State Commun. **58**, 507 (1986).
[25] T. Takimoto and T. Moriya, Solid State Commun. **99**, 457 (1996).
[26] C. L. Lin, J. Teter, J. E. Crow, T. Mihalisin, J. Brooks, A. I. Abou-Aly, and G. R. Stewart, Phys. Rev. Lett. **54**, 2541 (1985); J. McDonough and S. R. Julian, Phys. Rev. B **53**, 14411 (1996).
[27] F. Lapierre, P. Haen, A. Briggs, and M. Sera, J. Magn. Magn. Mater. **63&64**, 76 (1987).
[28] S. Paschen, E. Felder, and H. R. Ott, Eur. Phys. J. B **2**, 169 (1998).
[29] J. L. Gavilano, P. Vonlanthen, B. Ambrosini, J. Hunziker, F. Hulliger, and H. R. Ott, Europhys. Lett. **32**, 361 (1995).
[30] T. Cichorek (private communication).
[31] R. Marazza, D. Rossi, and R. Ferro, J. Less-Common Met. **75**, 25 (1980).
[32] P. Bonville, J. Hammann, J. A. Hodges, P. Imbert, and G. J. Jehanno, Phys. Rev. Lett. **57**, 2733 (1986).
[33] W. G. Marshall (unpublished).
[34] F. Merlo, M. Pani, and M. L. Fornasini, J. Alloys Compd. **221**, 280 (1995).
[35] C. Schank, U. Tegel, R. Henseleit, A. Grauel, G. Olesch, C. Geibel, G. Cordier, R. Kniep, and F. Steglich, J. Alloys Compd. **207/208**, 333 (1994).
[36] Z. Fisk and M. B. Maple, J. Alloys Compd. **183**, 303 (1992).
[37] M. Lenkewitz, S. Corsépius, and G. R. Stewart, J. Alloys Compd. **241**, 121 (1996).
[38] Ch. D. Routsi, J. K. Yakinthos, and H. Gamari-Seale, J. Magn. Magn. Mater. **117**, 79 (1992).
[39] P. Bonville, G. LeBras, P. Dalmas de Réotier, A. Yaouanc, R. Calemczuk, C. Paulsen, M. Kasaya, and F. G. Aliev, Physica B **230-232**, 266 (1997) and references cited therein.
[40] H. Kadowaki, T. Ekino, H. Iwasaki, T. Takabatake, H. Fujii, and J. Sakurai, J. Phys. Soc. Jpn. **62**, 4426 (1993).
[41] A. Dönni, H. Kitazawa, P. Fischer, J. Tang, M. Kohgi, Y. Endoh, and Y. Morii, J. Phys.: Condens. Matter **7**, 1663 (1995).
[42] K. Drescher, M. M. Abd-Elmeguid, H. Micklitz, J. P. Sanchez, C. Geibel, and F. Steglich, J. Magn. Magn. Mater. **182**, L275 (1998).
[43] K. Drescher, M. M. Abd-Elmeguid, H. Micklitz, and J. P. Sanchez, Phys. Rev. Lett. **77**, 3228 (1996).
[44] G. Ehlers and H. Maletta, Z. Phys. B **99**, 145 (1996).